Hindawi Publishing Corporation
Mathematical Problems in Engineering
Volume 2011, Article ID 327170, 20 pages
doi:10.1155/2011/327170

Research Article

Interior Noise Prediction of the Automobile Based on Hybrid FE-SEA Method

S. M. Chen,[1,2] D. F. Wang,[1,2] and J. M. Zan[3]

[1] *State Key Laboratory of Automotive Simulation and Control, Jilin University, Changchun 130022, China*
[2] *College of Automobile Engineering, Jilin University, No. 5988 Renmin Street, Changchun 130022, China*
[3] *State Key Laboratory of Vehicle NVH and Safety Technology, Chongqing 401120, China*

Correspondence should be addressed to D. F. Wang, caewdf@jlu.edu.cn

Received 6 May 2011; Accepted 11 July 2011

Academic Editor: Delfim Jr. Soares

In order to predict the interior noise of the automobile in the low and middle frequency band in the design and development stage, the hybrid FE-SEA model of an automobile was created using hybrid FE-SEA method. The modal density was calculated using analytical method and finite element method; the damping loss factors of the structural and acoustic cavity subsystems were also calculated with analytical method; the coupling loss factors between structure and structure, structure and acoustic cavity were both calculated. Four different kinds of excitations including road excitations, engine mount excitations, sound radiation excitations of the engine, and wind excitations are exerted on the body of automobile when the automobile is running on the road. All the excitations were calculated using virtual prototype technology, computational fluid dynamics (CFD), and experiments realized in the design and development stage. The interior noise of the automobile was predicted and verified at speed of 120 km/h. The predicted and tested overall SPLs of the interior noise were 73.79 and 74.44 dB(A) respectively. The comparison results also show that the prediction precision is satisfied, and the effectiveness and reliability of the hybrid FE-SEA model of the automobile is verified.

1. Introduction

Statistical Energy Analysis (SEA) method is widely used by many automobile industries and institutes to model automotive vibroacoustic system at high frequencies [1–4]. The subsystems with many modes show a short wavelength behavior and suit the application of the SEA method. At low frequencies, the assumptions of random resonance frequencies and mode shapes become less useful. The subsystems with few modes display a long wavelength behavior, and they are usually modeled using Finite Element Method (FEM). In order to deal with low and middle frequencies, a hybrid modeling method including finite element and statistical energy analysis (Hybrid FE-SEA) is used to develop the vibroacoustic model of the automobile system [5–9]. Meanwhile, the finite element method is a deterministic method,

and the SEA is a statistical method, the hybrid FE-SEA method combines two different methods to produce noniterative hybrid method which includes equations of dynamic equilibrium and power balance.

Langley [10–13] has an important contribution to the development of the hybrid FE-SEA method. And with the development of the hybrid FE-SEA method; it is widely used in automobile industry gradually. Charpentier et al. [14] predicted the structure-borne noise transmission in a trimmed automotive vehicle. And then, he also improved the design for interior noise using a hybrid FE-SEA model of a trimmed vehicle. And the sample prediction results illustrating the impact of design changes on interior noise level were shown along with the experimental validation result [15]. Musser and Rodrigues [16] improved the mid-frequency prediction accuracy for fully trimmed vehicle using hybrid FE-SEA technique. Shorter et al. [17] predicted and diagnosed component transmission loss using the hybrid FE-SEA method. Cotoni et al. [18] built a model of aircraft to predict the interior noise using the hybrid FE-SEA method, and it was demonstrated that the hybrid FE-SEA method can be successfully used to improve SEA models by including some details to the model that affect the vibroacoustic performance of the system. Manning [19] explored the hybrid method to expand SEA to the mid- and low frequency range where the assumption of high modal density is not valid. Cordioli et al. [20] investigated the acoustic performance of various slits using fast 3D numerical models based on the hybrid FE-SEA method, and the numerical investigation of the transmission loss of the seals and slits was performed for airborne SEA predictions.

In this research, a simplified hybrid FE-SEA model was built to predict the automobile interior noise. It is not the normal prediction with some experiments, but the interior noise was predicted at the development and design stage of the automobile. It is based on the prediction of the parameters and excitations. The parameters include modal density, damping loss factor, and coupling loss factor, and the excitations incorporate sound excitation of engine cabin, excitation of engine mounts, excitation of road roughness, and wind excitations.

2. Principle of Hybrid FE-SEA Method

The degrees of freedom q for one of the subsystems describe the displacement on the boundary. The relationship between q and a corresponding set of external forces f acting at the boundary can be written as:

$$f = Dq, \tag{2.1}$$

where D is the frequency-dependent dynamic stiffness matrix.

Formula (2.1) can be derived as

$$f_{\text{rev}} = D_{\text{dir}}q - Dq, \tag{2.2}$$

where D_{dir} is the "direct field" dynamic stiffness matrix and f_{rev} is "reverberant" force.

Formula (2.2) is substituted into Formula (2.1), and the new equation can be written as:

$$f_{\text{rev}} + f = D_{\text{dir}}q \tag{2.3}$$

The correlation between the response at node j of structure and node k of acoustic cavity can be written as

$$S_{qq} = -\left(\frac{4E}{\pi\omega n}\right)\mathrm{Im}\{H_{\mathrm{dir}}\} \Longrightarrow E\left[q_j q_k^*\right] = -\left(\frac{4E}{\pi\omega n}\right)\mathrm{Im}\{G(r_{jk})\}, \tag{2.4}$$

where H_{dir} is receptance matrix, and it is also the inverse of D_{dir}, E is the vibrational energy of the structural subsystem, G is the Green function, and r_{ij} is the distance between the grid points i and j. ω is the angular frequency, and n is the modal density of subsystem.

The hybrid FE-SEA equation can be written as

$$\begin{aligned}
&\sum_k \omega\eta_{jk}n_j\left(\frac{E_j}{n_j} - \frac{E_k}{n_k}\right) + \omega E_j\left(\eta_j + \eta_{dj}\right) = P_j + P_{\mathrm{in},j}^{\mathrm{ext}}, \quad j = 1,2,3\ldots,\\
&\omega\eta_{dj} = \left(\frac{2}{\pi n_j}\right)\sum_{r,s}\mathrm{Im}\ \{D_{d,rs}\}\left(D_{\mathrm{tot}}^{-1}\,\mathrm{Im}\left\{D_{\mathrm{dir}}^{(j)}\right\}D_t^{-1^*T}\right)_{rs}\\
&\omega\eta_{jk}n_j = \left(\frac{2}{\pi}\right)\sum_{r,s}\mathrm{Im}\left\{D_{\mathrm{dir},rs}^{(j)}\right\}\left(D_t^{-1}\,\mathrm{Im}\left\{D_{\mathrm{dir}}^{(j)}\right\}D_t^{-1^*T}\right)_{rs}\\
&P_{\mathrm{in},j}^{\mathrm{ext}} = \left(\frac{\omega}{2}\right)\sum_{r,s}\mathrm{Im}\left\{D_{\mathrm{dir},rs}^{(j)}\right\}\left(D_t^{-1}S_{ff}D_t^{-1^*T}\right)_{rs},
\end{aligned} \tag{2.5}$$

where η_j is the damping loss factor of the subsystem j, P_j is the input power of subsystem j, $P_{\mathrm{in},j}^{\mathrm{ext}}$ is the power that arises from forces applied to the deterministic system, η_{jk} is the coupling loss factor between subsystem j and k, n_j is the modal density of subsystem j, and S_{ff} is the cross-spectrum of the forces applied to the deterministic system.

3. Hybrid FE-SEA Model of the Automobile

The finite element model of the body in white (BIW) of the passenger automobile was created. The model is shown in Figure 1, and it includes 249481 nodes and 249963 elements. The mesh was mainly generated using quadrilateral elements, and some triangular elements are also included in the finite element model.

According to the finite element model of the body in white of the passenger automobile, a hybrid FE-SEA model was built. The subsystems of the hybrid FE-SEA model must be divided into FE subsystems or SEA subsystems. The large plate subsystems can be divided into SEA subsystems due to the high density such as roof, front and rear windshields, window glasses, and floor, and the beam-type subsystems can be divided into FE subsystems, such as A-pillar, B-pillar, C-pillar, and subframe. The division and properties of the subsystems of the hybrid FE-SEA model are shown in Table 1. Then, according to the nodes and elements of the FE model, the FE subsystems were created in the hybrid FE-SEA model, such as shock tower and longitudinal beams. Also, the SE subsystems were built based on the nodes from FE subsystems, such as roof and engine hood. The subsystems must be connected between FE and SE subsystems, FE and FE subsystems, and SE and SE subsystems in order to ensure that energy can transfer between connected subsystems. The last step of the modeling is to apply external excitations to the hybrid FE-SEA model.

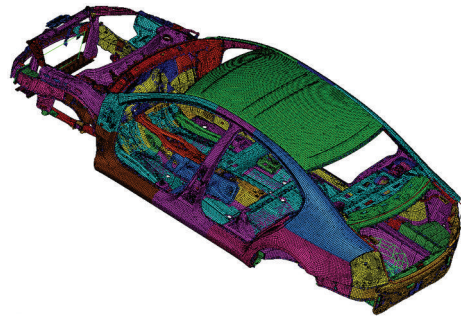

Figure 1: Finite element model of the body in white.

Table 1: Subsystem division and properties of the hybrid FE-SEA model.

Subsystem	Property	Subsystem	Property
Left-front door	SE curved plate	Right-front door	SE curved plate
Left-rear door	SE curved plate	Right-rear door	SE curved plate
Left-front window glass	SE plate	Right-front window glass	SE plate
Left-rear window glass	SE plate	Right-rear window glass	SE plate
Front windshield	SE plate	Rear windshield	SE plate
Front floor	SE plate	Rear floor	SE plate
Left-rear side wall	SE curved plate	Right-rear side wall	SE curved plate
Left A-pillar	FE	Right A-pillar	FE
Left B-pillar	FE	Right B-pillar	FE
Left C-pillar	FE	Right C-pillar	FE
Left-front fender	SE curved plate	Right-front fender	SE curved plate
Left-rear fender	SE curved plate	Right-rear fender	SE curved plate
Left-front mudguard	SE curved plate	Right-front mudguard	SE curved plate
Left-rear mudguard	SE curved plate	Right-rear mudguard	SE curved plate
Left-front shock tower	FE	Right-front shock tower	FE
Front bumper	SE curved plate	Rear bumper	SE curved plate
Left longitudinal beam	FE	Right longitudinal beam	FE
Subframe	FE	Firewall	FE
Trunk	SE curved plate	Engine hood	SE plate
Roof	SE curved plate	Trunk floor	SE plate
Passenger compartment cavity	SE cavity	Trunk cavity	SE cavity

The hybrid FE-SEA model is shown in Figure 2. It contains 89605 nodes. The hybrid FE-SEA is 159876 nodes less than the body in white of the automobile. Meanwhile, the whole body of the automobile including windshields, and doors contains 336305 nodes, and the hybrid FE-SEA model is 246700 nodes less than the whole body of the automobile. The acoustic cavities in the hybrid FE-SEA model are shown in Figure 3.

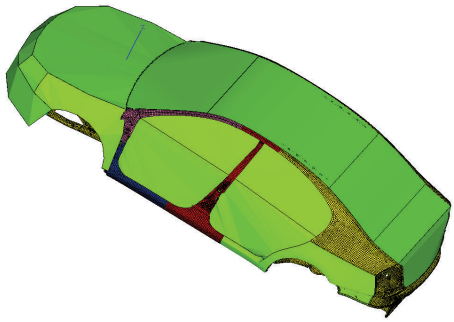

Figure 2: Hybrid FE-SEA model of the automobile.

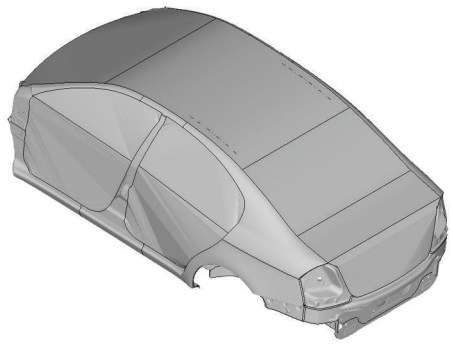

Figure 3: Acoustic cavities in the hybrid FE-SEA model.

4. Parameters of the Hybrid FE-SEA Model

4.1. Modal Density

In the hybrid FE-SEA model of automobile, FE subsystems and SE subsystems are included in the model. The SE subsystems can be simplified into regularly shaped plate. The modal densities of the SE subsystems such as roof, engine hood, trunk, and windows can be calculated with following equation:

$$n(f) = \frac{A_p}{2RC_l}, \tag{4.1}$$

where A_p is the area of the two-dimensional flat plate, R is radius of gyration, and C_l is longitudinal wave velocity. Some flat plates and curved plates were simplified to flat plates, and the modal densities of the SE subsystems are shown in Table 2.

The modal density is defined as

$$n(f) = \frac{N}{f_u - f_d}, \tag{4.2}$$

Table 2: Modal densities of the subsystems simplified to flat plates.

No.	SE subsystem	Property	Simplified	Modal density (Hz^{-1})
1	Front windshield	SE plate	Flat plate	0.0747
2	Rear windshield	SE plate	Flat plate	0.0781
3	Roof	SE curved plate	Flat plate	0.8422
4	Left-front window	SE plate	Flat plate	0.0305
5	Left-rear window	SE plate	Flat plate	0.0299
6	Right-front window	SE plate	Flat plate	0.0306
7	Right-rear window	SE plate	Flat plate	0.0300
8	Trunk	SE curved plate	Flat plate	0.3699
9	Engine hood	SE plate	Flat plate	0.4995

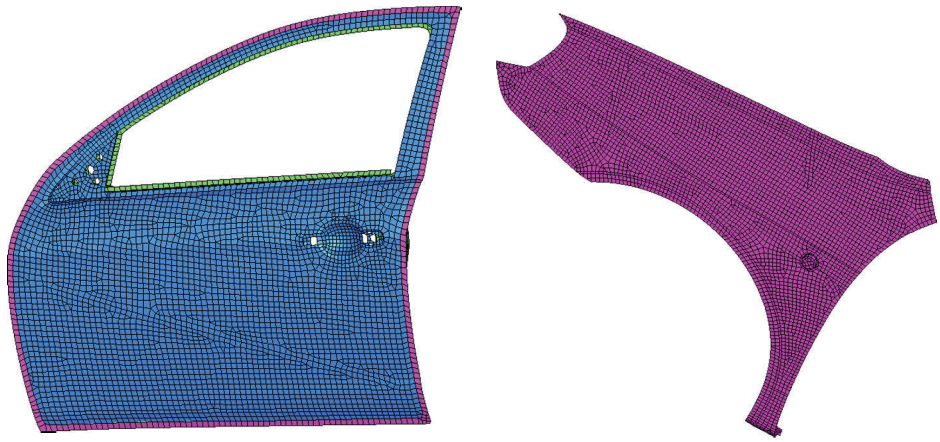

(a) Left-front door (b) Left-front fender

Figure 4: Finite element models of the subsystems.

where N is the mode numbers between f_u and f_d, f_u is the upper limit frequency of 1/3 octave band, f_d is the lower limit frequency of 1/3 octave band, and f is the center frequency of 1/3 octave band.

The modal densities of the FE subsystems and complicated SE subsystems can be calculated by formula (4.2). The modal densities of the FE subsystems can be calculated through finite element analysis. In order to obtain the modal information of the subsystems, finite element models of the subsystems in the hybrid FE-SEA model were created, and the left-front door and left-front fender are shown in Figure 4. Meanwhile, the modal analysis was performed for the finite element subsystem models. The modal density of the A-pillar is shown in Figure 5. The maximal modal density of the A-pillar is 0.1370 Hz^{-1} at 31.5 Hz. Three zero points of the modal density are at 20, 25, and 50 Hz, respectively. The modal density of the A-pillar increases from 63 to 1000 Hz in the view of the overall curve.

Taking spatial acoustic field of a cuboid with rigid walls $(r_1, r_2, r_3, 0 \le x_i \le r_i,\ i = 1, 2, 3)$ into consideration, it is assumed that the energy will not be loss, and the sound pressure can be written as

$$p = P\varphi(x_1, x_2, x_3)e^{i\omega t}, \tag{4.3}$$

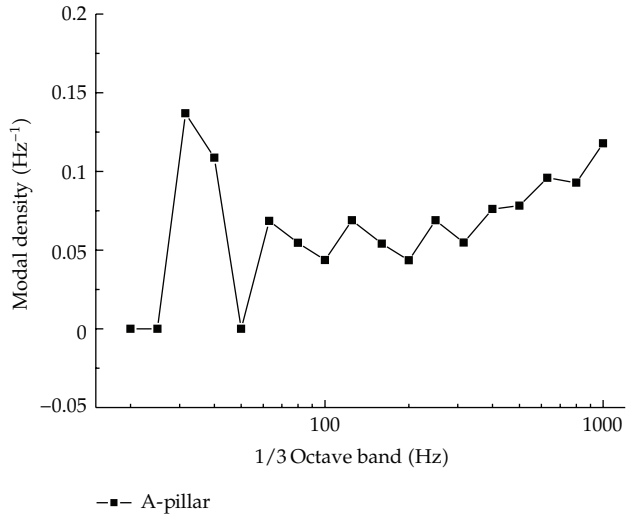

Figure 5: Modal density of the A-pillar.

where P is the amplitude of the sound pressure and $\varphi(x_1, x_2, x_3)$ is the acoustic mode function. The sound pressure is satisfied with wave equation and the condition of rigid walls:

$$\left(\frac{\partial^2}{\partial x_1^2} + \frac{\partial^2}{\partial x_2^2} + \frac{\partial^2}{\partial x_3^2}\right)\varphi + k^2\varphi = 0,$$
$$\frac{\partial \varphi}{\partial x_i} = 0, \tag{4.4}$$

where k is wave number, and $k = \omega/c$, ω is the circular frequency, and c is the sound speed. The mode number can be given by

$$N(k) = \frac{k^3 V_0}{6\pi^2}, \tag{4.5}$$

where V_0 is the volume of the acoustic field.

The modal density of the acoustic cavity can be expressed as

$$n(k) = \frac{k^2 V_0}{2\pi^2},$$
$$n(\omega) = \frac{\omega^2 V_0}{2\pi^2 c}. \tag{4.6}$$

Taking the influence of the surface area and total length of edges of the acoustic field on the modal density into account, the modal density of the acoustic cavity can be expressed as

$$n(\omega) = \frac{\omega^2 V_0}{2\pi^2 c^3} + \frac{\omega^2 A_s}{16\pi c^2} + \frac{\omega l_r}{16\pi c}, \tag{4.7}$$

where A_s is the surface area of the acoustic cavity and l_r is the total length of the edges.

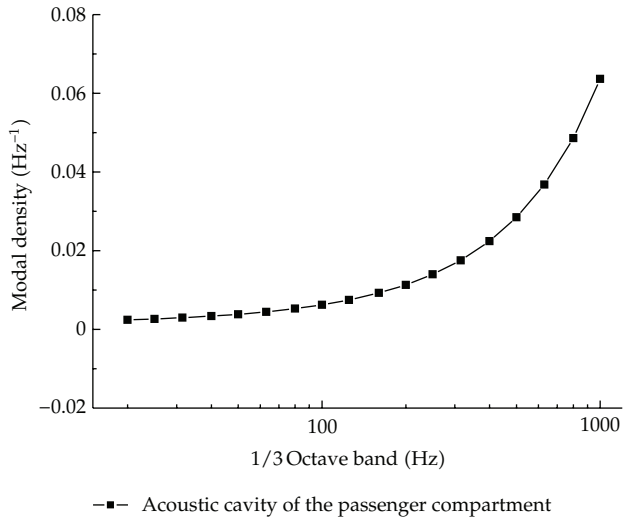

Figure 6: Modal density of the acoustic cavity of the passenger compartment.

The modal density of the acoustic cavity of the passenger compartment is shown in Figure 6. It increases as the frequency increases. The maximal modal density is 0.0636 Hz^{-1} at 1000 Hz.

4.2. Damping Loss Factor

Damping loss factor (DLF) is the rate of dissipative losses of subsystem energy. It is composed of three independent damping mechanisms, and it can be written as

$$\eta = \eta_s + \eta_r + \eta_b, \tag{4.8}$$

where η_s is the structural loss factor consisted of material inner friction of subsystem, and η_r is the loss factor formed by acoustic radiation of subsystem, η_b is the loss factor formed by border connection damping among subsystems.

Structural loss factor is relative to material performance. The different subsystems of vehicle body are mainly composed of steel, glass, and engineering plastics. The structural loss factors of some common materials are shown in Table 3.

Damping loss factor of acoustic radiation η_r can be expressed as

$$\eta_r = \frac{\rho_0 c \sigma}{\omega \rho_s}, \tag{4.9}$$

where ρ_0 is air density, c is sound speed, ρ_s is area density of structure, and σ is the radiation ratio of the structure.

Additionally, η_b is extremely small. Thus, it can be ignored. The damping loss factor of the front floor is shown in Figure 7. The DLF of the front floor decreases as the frequency increases. The maximum and minimum values of the damping loss factors of the front floor are 0.0172 and 0.0030, respectively.

Table 3: Structural loss factors of some common used materials.

Material	Structural loss factor η_s
Steel	3×10^{-4}
Glass	1×10^{-3}
Engineering plastics	0.3
Aluminum	1×10^{-4}
Brass	2×10^{-3}
Cast iron	1×10^{-3}
Plywood	1.5×10^{-2}
PVC	0.3

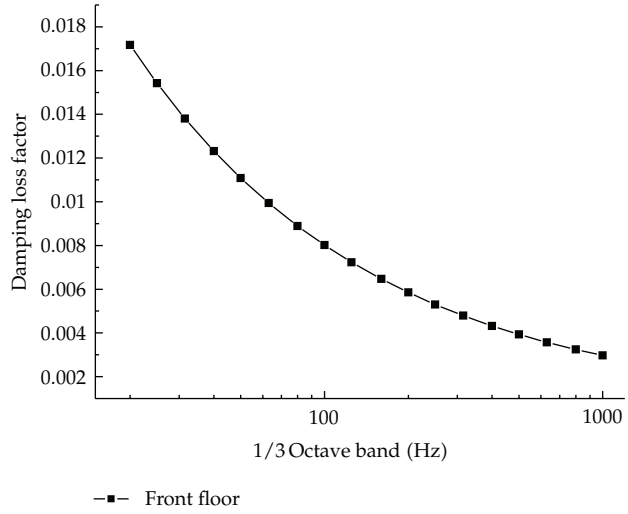

Figure 7: Damping loss factor of the front floor.

The interior acoustic cavity can be regarded as semifree sound field. Meanwhile, the sound absorption coefficient of the interior acoustic cavity of the automobile can be obtained in acoustics handbooks. The relationship between the damping loss factor and sound absorption coefficient of the interior acoustic cavity of the automobile can be expressed as

$$\eta_{\text{ac}} = \frac{\alpha c S}{8\pi f V}, \tag{4.10}$$

where η_{ac} is damping loss factor, α is sound absorption coefficient, S is the surface area of sound cavity, c is the velocity of sound, f is the center frequency of 1/3 octave band, and V is the volume of sound cavity.

The damping loss factor of the acoustic cavity of the passenger compartment is shown in Figure 8. It fluctuates between 0.0001 and 0.0005. The minimum and maximum damping loss factors of the acoustic cavity of the passenger compartment are 0.00012 and 0.00042 at 1000 and 80 Hz, respectively.

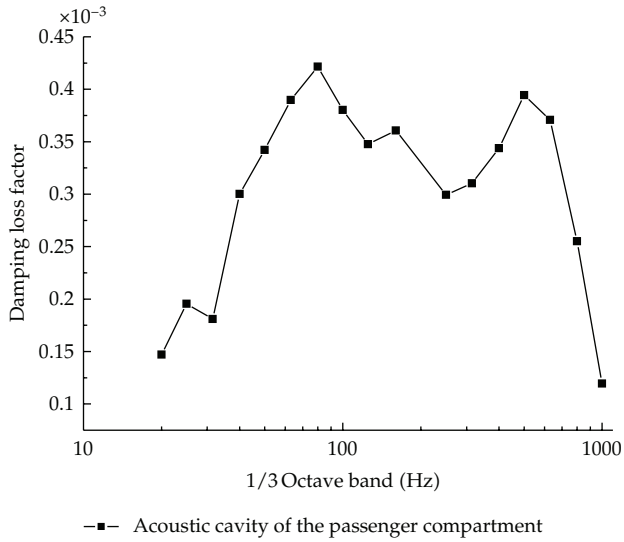

Figure 8: Damping loss factor of the acoustic cavity of the passenger compartment.

4.3. Coupling Loss Factor

It is assumed that subsystem i and subsystem j are connected with a line. Meanwhile, the length of the coupling line is far more than the wave length of the free wave in the subsystems. Linear connection among the structural subsystems is the most common junction form in structure-structure coupling of the automobile body, and the coupling loss factor (CLF) of linear connection between subsystems i and j can be described as:

$$\eta_{ij} = \frac{lc_g}{\pi\omega A_i}\langle\tau_{ij}\rangle, \tag{4.11}$$

where l is the length of coupling line, c_g is bending wave velocity of subsystem, A_i is surface area of subsystem i, and τ_{ij} is the wave transmission coefficient from subsystem i to j. The CLFs between firewall and front floor are shown in Figure 9.

Structure-cavity coupling is also a kind of common connection form between structural subsystem and acoustic cavity. The coupling loss factors from structural subsystem to acoustic cavity can be depicted as:

$$\eta_{\mathrm{sc}} = \frac{\rho_0 c\sigma}{\omega\rho_s}, \tag{4.12}$$

where ρ_0 is the density of air, σ is the sound radiation coefficient, c is the sound speed, ρ_s is the area density of structure, and ω is the circular frequency.

According to the reciprocity theorem, CFL from cavity to structural subsystem can be written as

$$\eta_{\mathrm{cs}} = \frac{\sigma\rho_0 c n_s}{\omega\rho_s n_c}, \tag{4.13}$$

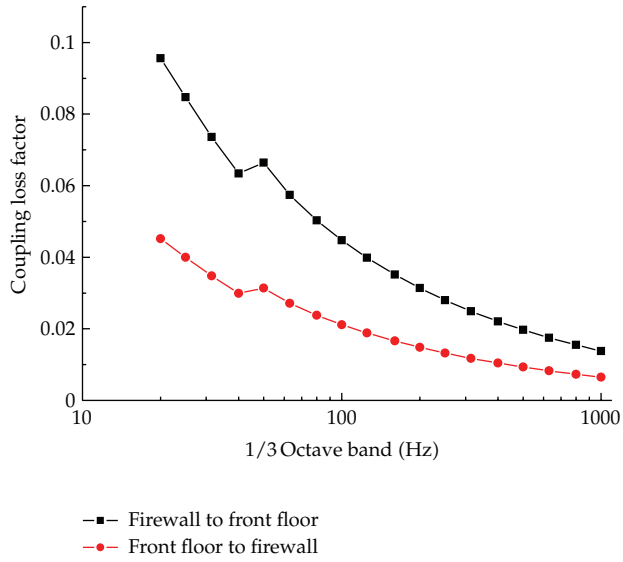

Figure 9: CLFs between firewall and front floor.

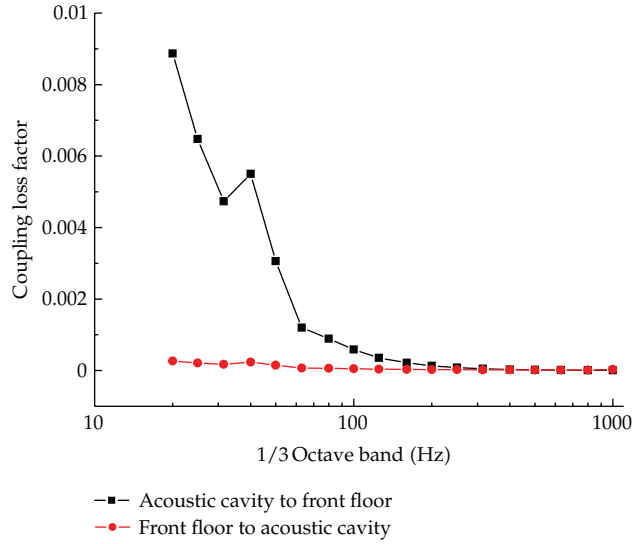

Figure 10: CLFs between acoustic cavity and front floor.

where n_s is the modal density of structural subsystem and n_c is the modal density of acoustic cavity.

The CLFs between acoustic cavity and front floor are shown in Figure 10. The CLFs from acoustic cavity to front floor are basically larger than the corresponding values from front floor to acoustic cavity. The CLFs from front floor to acoustic cavity are extremely small, and their values are smaller than 0.0003. The maximum CLF from acoustic cavity to front floor is0.0089.

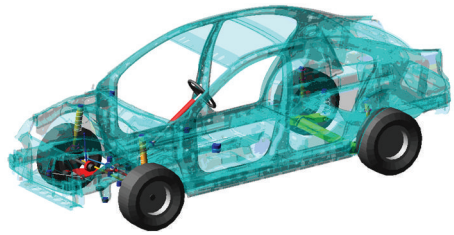

Figure 11: Rigid-elastic coupling multibody dynamics model.

5. Excitations of Hybrid FE-SEA Model

Vehicle body is excited when it is running on the road. There are four basic excitations including road excitation, engine mount excitation, sound radiation excitation of engine, and wind excitation. The excitations can be obtained through different method during the development and design stage of the automobile.

5.1. Road Excitations

The body of the automobile is excited by road when the automobile is running, and the road excitation acts through tyre, front and rear suspensions. Physical prototype of an automobile is not available to measure road excitation during the design and development stage of automobile. As the development of the virtual prototype technology, the virtual prototype model of an automobile can be created during the design and development stage. In order to obtain the road excitation, a multibody system model of the automobile was built according to the basic parameters of the chassis and body systems. Taking the effect of elastic body on the precision of the road excitation into consideration, a rigid-elastic coupling multibody dynamics model was built using mode synthesis method. The rigid-elastic coupling model is shown in Figure 11.

The rigid-elastic coupling model was driven on B-level road at 120 km/h. The excitations were measured at front shock towers and rear shock towers of spring and damping shock absorbers, respectively. A total of six excitation points were included in the model, and they were left-front shock tower, right-front shock tower, left-rear shock towers of spring and damping shock absorber, and right-rear shock towers of spring and damping shock absorber. The road excitations are shown in Figure 12. They fluctuate from 20 to 1000 Hz. The minimum and maximum road excitations are 0.0353 and 0.2006 m/s^2 at 400 and 50 Hz, respectively, for right-front shock tower. The first three maximum values are 0.4305, 0.2553, and 0.2006 m/s^2 for left-front shock tower, left-rear damping, and right-front shock tower, respectively.

5.2. Engine Mount Excitations

The excitation of engine mounts to body also cannot be measured during the design and development stage before prototype manufactured. The layout of automobile must be confirmed at the beginning of the design and develop stage. Then, the engine and its mounts of the designed automobile also can be determined. The excitations of engine mounts to body can be obtained through engine rig test.

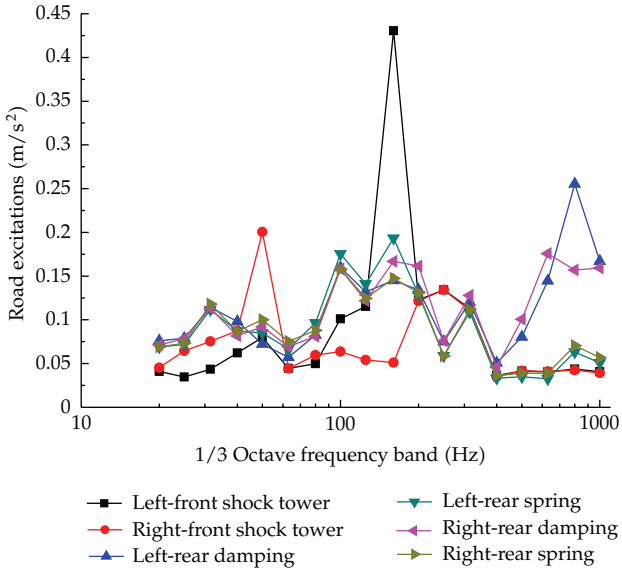

Figure 12: Road excitations.

The running speed of the vehicle was 120 km/h, and it was equal to 3200 r/min of the engine speed. In order to acquire the excitations at the passive sides of the engine mounts, an experiment was presented on the test rig in a semianechoic room. The engine was installed on a dynamometer. Because the engine mount system was comprised of four engine mounts including front mount, left mount, right mount, and rear mount, four accelerometers were installed in on the initiative sides of the engine mounts. Finally, the vibration accelerations at four different mounts were measured at speed of 3200 r/min. The relationship between the accelerations at initiative and passive sides of the engine mount can be written as

$$T = 20 \log \frac{|a_u|}{|a_d|}, \tag{5.1}$$

where T is the transmissibility of the engine mount, a_u is the vibration acceleration of the engine mount at initiative side, and a_d is the acceleration of the engine mount at passive side.

The acceleration at initiative side a_u was measured, and the transmissibility of the mount T was known. The acceleration at passive side a_d can be calculated as follows:

$$|a_d| = \frac{|a_u|}{10^{T/20}}. \tag{5.2}$$

The excitations of the engine mounts were calculated according to formula (5.2). The excitations of the engine mounts are shown in Figure 13. For the front engine mount, it is nearly horizontal from 20 to 100 Hz; it fluctuates up and down from 125 to 1000 Hz; the maximum acceleration of the front engine mount is 1.9640 m/s^2 at 400 Hz. The values of the excitation of the left engine mount are extremely small. It is strongly fluctuated from 80 Hz to 800 Hz for right engine mount, the maximum value of which is 10.0879 m/s^2 at 400 Hz. Meanwhile, the maximum value of the excitation of the rear engine mount is 1.3984 m/s^2 at 500 Hz.

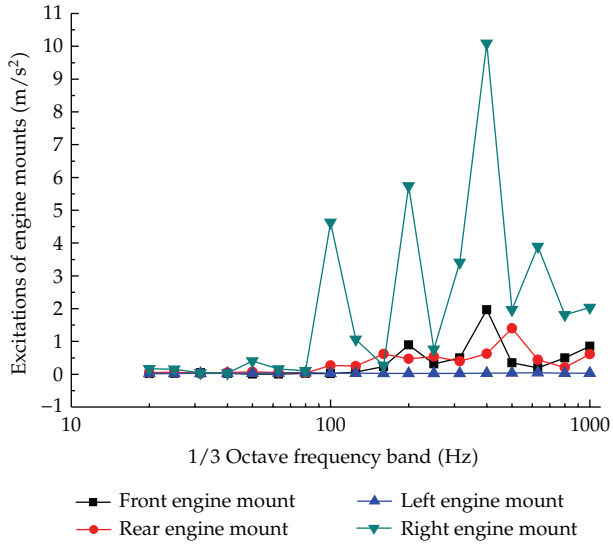

Figure 13: Excitations of engine mounts.

5.3. Sound Radiation Excitations of the Engine

Sound radiation excitation of engine cabin received by engine cabin panels is one of the most major excitations to the body of automobile. The measurement of the sound radiation excitation is not available during the design and development stage of automobile. However, it can be acquired throughout indoor testing according to ISO 6798: 1995 "Reciprocating internal combustion engines—Measurement of emitted airborne noise—Engineering method and survey method." Emitting sound power of the engine could be measured with engineering method. Meanwhile, on the basis of point sound source theory, sound radiation excitation of engine received by engine cabin panels can be calculated by the following equation:

$$L_{\text{se}} = L_e - 20 \log \frac{r_2}{r_1}, \tag{5.3}$$

where L_{se} is sound pressure level (SPL) of engine cabin inner surface; L_e is the measuring point SPL of engine sound power experiment; r_1 is the distance between measuring point and engine, generally, $r_1 = 1$; r_2 is the distance between prediction point and engine.

From formula (5.3), if L_e and r_2 are known, the sound excitation at every surface of engine cabin could be calculated.

The layout of the sound power test of the engine was the same as illustrated in Section 5.2. Nine microphones were placed at different positions according to ISO 6798: 1995 "Reciprocating internal combustion engines—Measurement of emitted airborne noise—Engineering method and survey method." The SPLs of the engine were measured at speed of 3200 r/min. The sound radiation excitation of the engine was calculated by formula (5.3). The sound excitations of the engine cabin are shown in Figure 14. For the left-front fender, it goes up gradually and fluctuates up and down from 20 to 1000 Hz; the minimum and maximum SPLs of the sound excitation of the left-front fender are 38.42 and 91.40 dB(A) at 20 and 500 Hz, respectively. The other four sound excitations were also applied on the right-front fender, engine hood, front bumper, and firewall, respectively. Meanwhile, these four

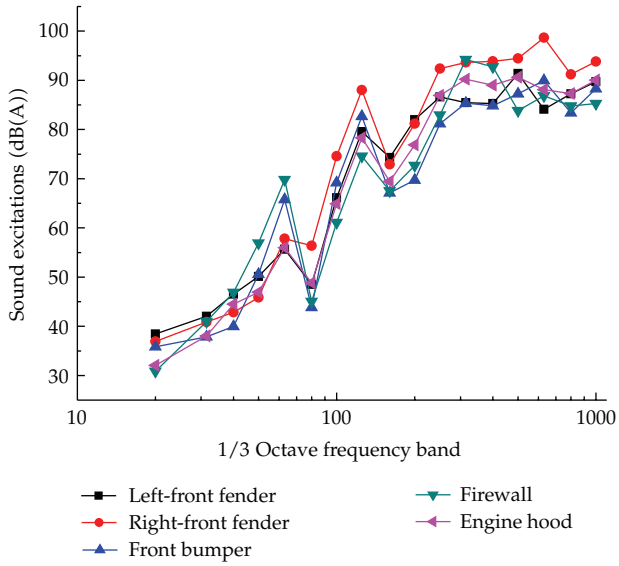

Figure 14: Sound excitations of the engine cabin.

sound excitations have the same trend, and the amplitudes of these four sound excitations are fluctuating near the sound excitation values of the left-front fender.

5.4. Wind Excitations

The body of automobile is excited by wind when the automobile is running on the road. Also, the wind excitation becomes a major noise source at high speeds. Wind excitations can be measured through wind tunnel test. However, the wind tunnel test is extremely expensive, and the wind excitations are not available without physical prototype of automobile during the design and development stage of automobile. For the purpose of acquiring the wind excitation, the Ffowcs Williams and Hawkings (FW-H) model was used with computational fluid dynamics (CFD) software of Fluent.

The Ffowcs Williams and Hawkings (FW-H) equation can be written as [21, 22]

$$\frac{1}{a_0^2}\frac{\partial^2 p'}{\partial t^2} - \nabla^2 p' = \frac{\partial^2}{\partial x_i \partial x_j}\left[T_{ij}H(f)\right] - \frac{\partial}{\partial x_i}\left\{\left[P_{ij}n_j + \rho u_i(u_n - v_n)\right]\delta(f)\right\} + \frac{\partial}{\partial t}\left\{\left[\rho_0 v_n + \rho(u_n - v_n)\right]\delta(f)\right\}, \tag{5.4}$$

where u_i is the fluid velocity component in the x_i direction, v_i is the surface velocity components in the x_i direction, u_n is the fluid velocity component normal to the surface $f = 0$, and $f = 0$ means a mathematical surface introduced to "embed" the exterior flow problem ($f > 0$) in an unbounded space, which facilitates the use of generalized function theory and the free-space Green function to obtain the solution. v_n is the surface velocity component normal to the surface, $H(f)$ is the Heaviside function, $\delta(f)$ is the Dirac delta function, p' is the sound pressure at the far field ($p' = p - p_0$), n_i is the unit normal vector pointing toward

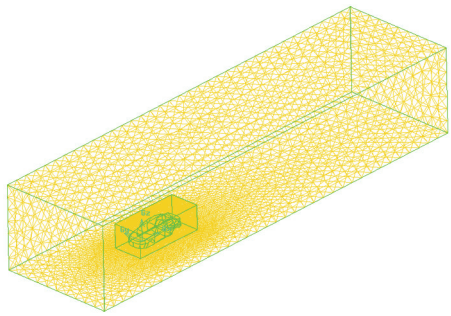

Figure 15: CFD model of the automobile.

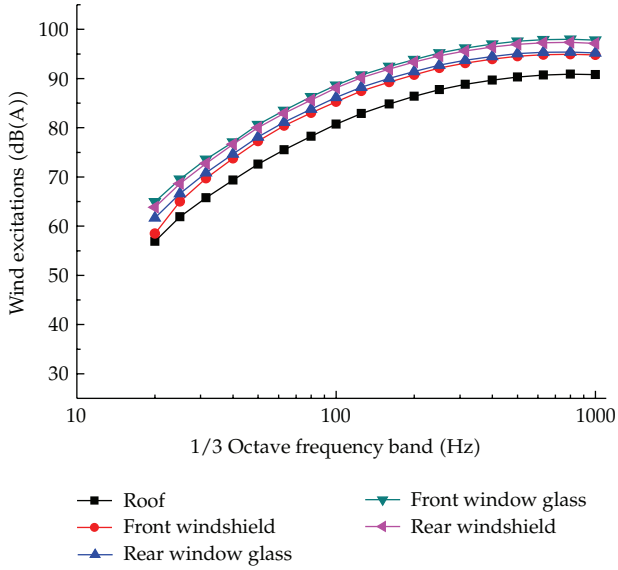

Figure 16: Wind excitations of the subsystems.

the exterior region, a_0 is the far-field sound speed, ρ is the density of air, T_{ij} is the Lighthill stress tensor, and P_{ij} is the compressive stress tensor.

The CFD model of the automobile was created according to the CFD method. The size of simulation wind tunnel in CFD model was 8 times length, 5 times width, and 5 times height of the automobile. The corresponding length, width, and height were 36400 mm, 9500 mm, and 7000 mm, respectively. TGrid-type grid was used in the CFD model which was divided into 233280 grids. The CFD model of the automobile is shown in Figure 15. The sound excitations were calculated at different body panels using large eddy simulation (LES). Three monitoring points were placed at every different body panel on the left half of body because of the symmetry of the automobile. The inlet velocity was set as 120 km/h, and the walls of the wind tunnel and the surfaces of the automobile were both set to walls. After the simulation, the wind excitations at three monitoring points of every body panel were averaged, and the averaged SPLs were the wind excitations of the automobile. The simulation results are validated by Yang's wind tunnel test [23]. The wind excitations of the

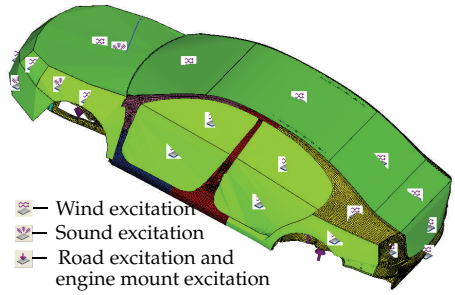

Figure 17: Hybrid FE-SEA model with parameters and excitations.

Figure 18: Microphone at driver's right ear position.

subsystems are shown in Figure 16. They go up until 800 Hz. The maximum wind excitation is front window glass, and the minimum and maximum values are 64.94 and 97.98 dB(A) at 20 and 800 Hz, respectively.

6. Interior Noise Prediction

All the input parameters including modal density, damping loss factors, and coupling loss factors were added in the hybrid FE-SEA model. Meanwhile, the excitations including road excitations, engine mount excitations, sound radiation excitations of the engine, and wind excitations were also excited on the hybrid FE-SEA model. Simultaneously, the sound absorption and insulation effects of the trimmed body were taken into consideration. The hybrid FE-SEA model with parameters and excitations is shown in Figure 17.

The interior SPL of the automobile was predicted at driver's right ear with the hybrid FE-SEA model. Meanwhile, in order to verify the correctness of the prediction results, the interior noise of the automobile was measured with a physical prototype vehicle on an asphalt road at speed of 120 km/h. A microphone shown in Figure 18 was placed at the side of driver's right ear. The interior noise signal was recorded using LMS SCADAS data acquisition front end. After data acquisition, the noise signal was processed by Fast Fourier Transform (FFT) and A-weighted network.

The comparison between the predicted and measured sound pressure levels of the automobile is shown in Figure 19. The SPL of the prediction fluctuates up and down around the corresponding value of the test, and it also shows a good agreement of experimentation

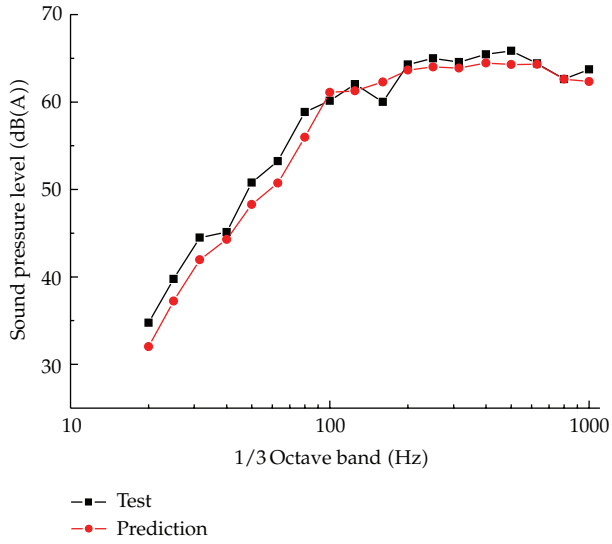

Figure 19: Comparison between sound pressure levels of prediction and test.

and prediction from 20 to 1000 Hz. The errors from 20 to 100 Hz are basically larger than the values from 200 to 1000 Hz. The minimum and maximum errors are 0.01 and 2.87 dB(A) at 800 and 160 Hz, respectively. The maximum absolute error is less than 3 dB(A). The overall A-weighted sound pressure levels of prediction and test are 73.79 and 74.44 dB(A), respectively. The absolute error is 0.65 dB(A), and the relative error is 0.87%. The overall relative error is less than 1%, and the absolute error is less than 1.0 dB(A). The comparison results also show that the prediction precision is satisfied, and the effectiveness and reliability of the hybrid FE-SEA model of the automobile are verified.

7. Conclusions

The hybrid FE-SEA method was used to predict interior noise of the automobile at the design and development stage in this paper. The hybrid FE-SEA model of the automobile was created using hybrid FE-SEA method. The parameters of the hybrid FE-SEA model including modal density, damping loss factor, and coupling loss factor were calculated using analytical and finite element methods. The excitations including road excitations, engine mount excitations, sound radiation excitations of the engine, and wind excitations were calculated using virtual technology and engine tests. All the parameters and excitations can be available at the design and development stage. Furthermore, the interior noise of the automobile was predicted and verified.

It is shown that the predicted SPLs of the interior noise have a good agreement with the corresponding values of the test. The predicted and tested overall SPLs of the interior noise were 73.79 and 74.44 dB(A), respectively. The absolute error is 0.65 dB(A), and the relative error is 0.87%. The overall relative error is less than 1%, and the absolute error is less than 1.0 dB(A). The comparison results also show that the prediction precision is satisfied, and the effectiveness and reliability of the hybrid FE-SEA model of the automobile is verified. The prediction of the interior noise of the automobile can be realized through various calculation methods, presented in this paper in the design and development stage.

Acknowledgments

This paper is supported by National Natural Science Foundation Project (no. 50975119) and National Key Technology R&D Program of China (no. 2011BAG03B01). The authors would like to express their appreciations for the above fund support.

References

[1] W. Jeong and K. Park, "Application of virtual SEA for the prediction of acoustic performance of cockpit," SAE Paper 2009-01-0767, 2009.

[2] R. Gujarathi, D. Copley, R. Romick et al., "Modeling interior noise in off-highway trucks using statistical energy analysis," SAE Paper 2009-01-2239, 2009.

[3] H. Uehara, T. Koizumi, N. Tsujiuchi et al., "Application of statistical energy analysis to noise prediction of co-generation system," in *Proceedings of the Small Engine Technology Conference*, SAE International Warrendale Pennsylvania, Milwaukee, Wis, USA, 2008.

[4] C. T. Musser and T. Bharj, "Component-level vehicle target setting using statistical energy analysis," in *Proceedings of the JSAE Spring Conference*, SAE International Warrendale Pennsylvania, Tokyo, Japan, 2008.

[5] P. J. Shorter and R. S. Langley, "Modeling structure-borne noise with the Hybrid FE-SEA method," in *Structural Dynamics—EURODYN 2005*, vol. 1–3, pp. 1205–1210, IOS Press, 2005.

[6] P. J. Shorter and R. S. Langley, "Vibro-acoustic analysis of complex systems," *Journal of Sound and Vibration*, vol. 288, no. 3, pp. 669–699, 2005.

[7] R. Rashid and R. S. Langley, "A hybrid method for modelling in-vehicle boom noise," in *Proceedings of the 2004 International Conference on Noise and Vibration Engineering, ISMA*, pp. 3487–3499, bel, September 2004.

[8] I. Vaz and J. Pan, "Vibro-acoustic modeling of the APAMAT II test system," SAE Paper 2009-01-2210, 2009.

[9] S. G. Mattson, D. Labyak, J. Pruetz, and T. Connelly, "Prediction of muffler insertion loss by a hybrid FE acoustic-SEA model," *SAE International Journal of Passenger Cars - Mechanical Systems*, vol. 2, no. 1, pp. 1323–1329, 2009.

[10] R. S. Langley and P. Bremner, "A hybrid method for the vibration analysis of complex structural-acoustic systems," *Journal of the Acoustical Society of America*, vol. 105, no. 3, pp. 1657–1671, 1999.

[11] R. S. Langley and J. A. Cordioli, "Hybrid deterministic-statistical analysis of vibro-acoustic systems with domain couplings on statistical components," *Journal of Sound and Vibration*, vol. 321, no. 3–5, pp. 893–912, 2009.

[12] R. S. Langley and V. Cotoni, "Response variance prediction for uncertain vibro-acoustic systems using a hybrid deterministic-statistical method," *Journal of the Acoustical Society of America*, vol. 122, no. 6, pp. 3445–3463, 2007.

[13] P. J. Shorter and R. S. Langley, "On the reciprocity relationship between direct field radiation and diffuse reverberant loading," *Journal of the Acoustical Society of America*, vol. 117, no. 1, pp. 85–95, 2005.

[14] A. Charpentier, P. Streedhar, and K. Fukui, "Using the hybrid FE-SEA method to predict structure-borne noise transmission in a trimmed automotive vehicle," SAE Paper 2007-01-2181, 2007.

[15] A. Charpentier, P. Sreedhar, G. Gardner et al., "Use of a hybrid FE-SEA model of a trimmed vehicle to improve the design for interior noise," SAE Paper 2009-01-2199, 2009.

[16] C. T. Musser and A. B. Rodrigues, "Mid-frequency prediction accuracy improvement for fully trimmed vehicle using hybrid SEA-FEA technique," SAE Paper 2008-36-0564, 2008.

[17] P. Shorter, Q. Zhang, and A. Parrett, "Using the hybrid FE-SEA method to predict and diagnose component transmission loss," SAE Paper 2007-01-2172, 2007.

[18] V. Cotoni, B. Gardner, J. A. Cordioli et al., "Advanced modelling of aircraft interior noise using the hybrid FE-SEA method," SAE Paper 2008-36-0575, 2008.

[19] J. E. Manning, "Hybrid SEA for mid-frequencies," SAE Paper 2007-01-2305, 2007.

[20] J. Cordioli, V. Cotoni, and P. Shorter, "Numerical investigation of the transmission loss of seals and slits for airborne SEA predictions," SAE Paper 2009-01-2205, 2009.

[21] J. E. Ffowcs Williams and D. L. Hawkings, "Sound generation by turbulence and surfaces in arbitrary motion," *Philosophical Transactions of the Royal Society of London. Series A*, vol. 264, no. 1151, pp. 321–342, 1969.

[22] K. S. Brentner and F. Farassat, "Analytical comparison of the acoustic analogy and Kirchhoff formulation for moving surfaces," *AIAA Journal*, vol. 36, no. 8, pp. 1379–1386, 1998.
[23] B. Yang, X. Hu, and Y. Zhang, "Study on unsteady flow field and aerodynamic noise of the automobile rear view mirror region," *Journal of Mechanical Engineering*, vol. 46, no. 22, pp. 151–155, 2010.